

# RepILN: Reparameterized Inertial Localization Network

Shanshan Zhang, Tianshui Wen, Siyue Wang, Qi Zhang, Ziheng Zhou, Lingxiang Zheng, Yu Yang

**Abstract**—Inertial localization is considered a promising solution for positioning consumer-grade IoT devices due to its cost-effectiveness and independence from external infrastructure. However, data-driven inertial localization approaches often rely on increasingly complex network architectures to improve accuracy, which poses challenges for the limited computational resources of IoT devices. Furthermore, these methods frequently neglect the importance of modeling long-term dependencies in inertial measurements—an essential aspect for accurate trajectory reconstruction—thereby limiting localization performance. To address these challenges, we propose a reparameterized inertial localization network that employs a multi-branch structure during training to enhance feature extraction. At inference time, this structure is transformed into an equivalent single-path architecture, improving parameter efficiency. To further capture long-term dependencies in motion trajectories, we introduce a temporal-scale sparse attention mechanism that selectively emphasizes key trajectory segments while suppressing noise. Additionally, a gated convolutional unit is incorporated to effectively integrate long-range dependencies with local fine-grained features. Extensive experiments on public benchmarks demonstrate that our method achieves a favorable trade-off between accuracy and model compactness. For instance, on the RoNIN dataset, our approach reduces the Absolute Trajectory Error (ATE) by 2.59% compared to RoNIN-ResNet, while also reducing the number of parameters by 3.86%.

**Index Terms**—IoT, Constrained Devices, IMU, Localization, Deep Learning

## I. INTRODUCTION

**I**NERTIAL localization aims to estimate position from inertial sensor measurements. Typically, these sensors consist of accelerometers and gyroscopes, providing direct measurements of acceleration and angular velocity. Due to their low power consumption, intrinsic data privacy, and immunity to environmental conditions, inertial sensors have found widespread applications in location-based services, assistive localization for disabled individuals, IoT device positioning, and ambient-assisted living [1]–[7]. Inertial localization methods are generally divided into two categories: Newtonian mechanics-based methods and data-driven methods.

Traditional methods based on Newtonian mechanics offer the advantage of low computational cost. However, they face issues such as the accumulation of errors [8] and noise and restrict the placement of inertial sensors while constraining movement patterns [9], [10], limiting their practicality in real-world applications.

Data-driven methods derive position estimates directly from sensor data, adapting to complex motion states and sensor configurations. For example, RoNIN [11] employs ResNet [12], LSTM [13], and temporal convolutional networks (TCN) [14] to estimate velocity. This unified inertial localization framework demonstrates strong robustness across diverse scenarios, laying the foundation for subsequent research. Building upon this, TLIO [15] integrates the stochastic-cloning

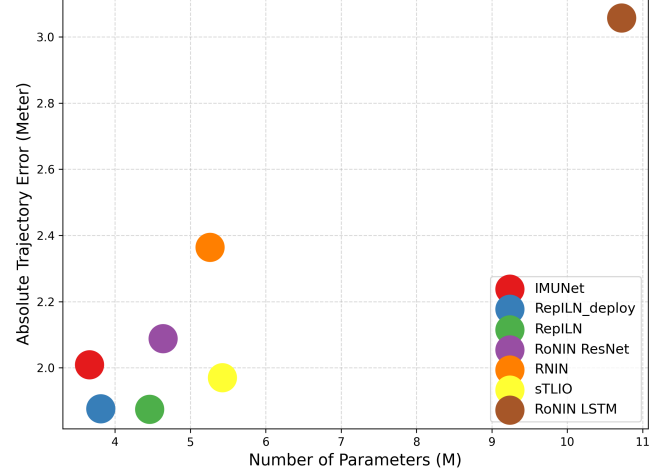


Fig. 1. Compares the ATE performance of different models on the RNIN-VIO dataset. Each point represents a model, where a position closer to the bottom-left corner indicates lower trajectory error and a smaller number of parameters, reflecting better overall efficiency. Our proposed RepILN and its reparameterized variant (RepILN\_deploy) strike a favorable balance between model size and localization accuracy.

extended Kalman filter (SCEKF) [16] with ResNet-inferred displacement to minimize trajectory errors. Similarly, RNIN-VIO [17] incorporates LSTM into ResNet to capture long-term dependencies in the trajectory. Additionally, IMUNet [18] utilizes depthwise separable convolutions (DSC) to construct a lightweight network optimized for mobile devices, and its performance is compared with MobileNet [19], MnasNet [20], and EfficientB0 [21].

Although data-driven methods have significantly advanced inertial localization by learning complex motion patterns from sensor data, several challenges remain. First, increasingly sophisticated network architectures often lead to higher computational costs and reduced parameter efficiency, making deployment on resource-constrained platforms—such as edge computing nodes and IoT devices—more challenging. Second, conventional models such as CNNs and LSTMs struggle to capture long-term dependencies effectively, thereby limiting further improvements in localization accuracy.

To address these limitations, we propose a reparameterized inertial localization network that efficiently models temporal dynamics and enhances position estimation performance from raw inertial sensor data. Experimental results on multiple public datasets demonstrate that the proposed method outperforms benchmark models while simultaneously achieving a favorable trade-off between accuracy and computational efficiency, as illustrated in Fig. 1. The main contributions of this paper are as follows:

- Reparameterizing the model during inference to decouple training from inference, thereby improving parameter

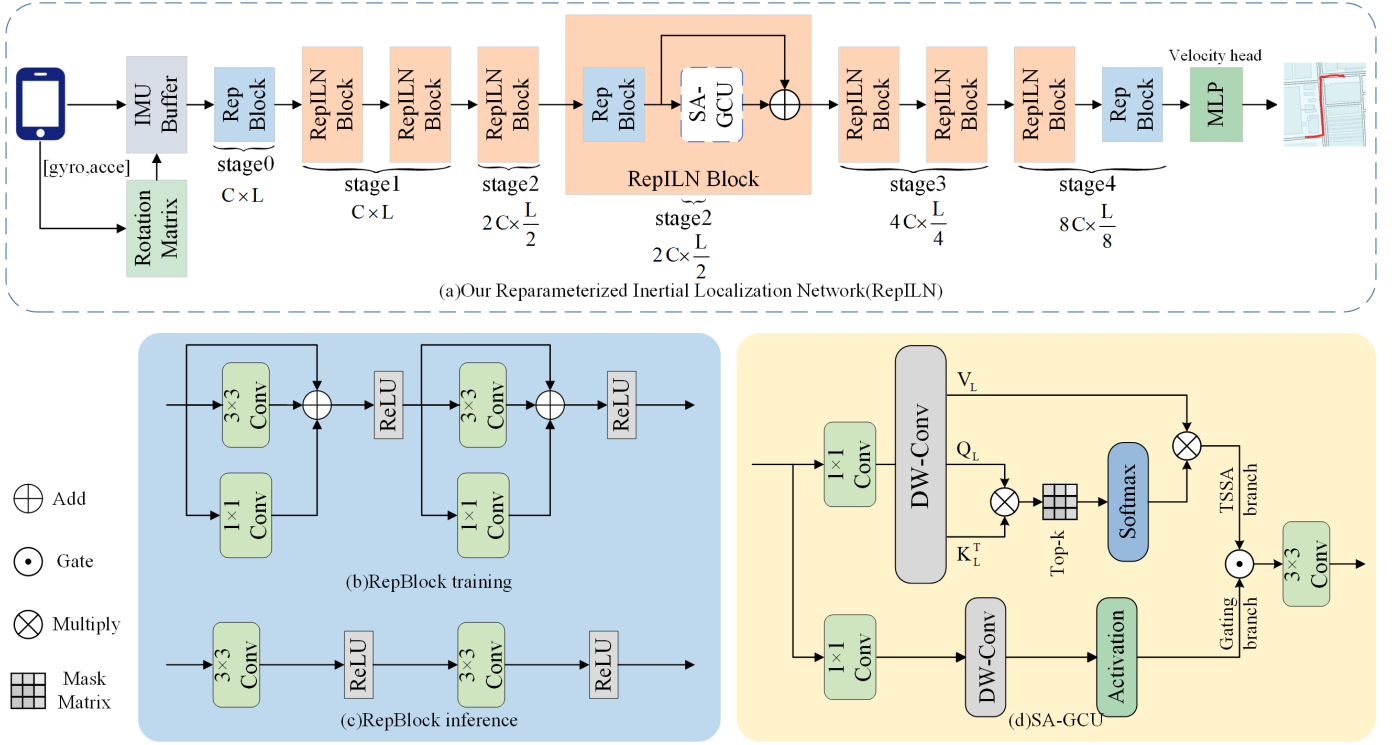


Fig. 2. The overall architecture of the proposed Reparameterized Inertial Localization Network (RepILN) consists of the Reparameterization Module (RepBlock) and the Sparse Attention Gated Convolutional Unit (SA-GCU), where the gating branch uses local fine-grained features to modulate the global representations extracted by the TSSA branch.

efficiency while maintaining a balance between accuracy and computational cost.

- Proposing a Temporal-Scale Sparse Attention (TSSA) mechanism that captures long-term trajectory dependencies while selectively preserving salient features and suppressing irrelevant noise.
- Introducing a Sparse Attention Gated Convolutional Unit (SA-GCU) to enable multi-scale feature modeling, where local fine-grained features are employed to gate and modulate the global representations extracted by the TSSA branch.

## II. RELATED WORK

### A. Inertial Localization Methods

Traditional inertial localization methods are typically based on Newtonian mechanics. For example, SINS [8] rotates the acceleration vector into a global coordinate system to compensate for gravity, and then estimates displacement through double integration. However, measurement noise continuously accumulates during this process, leading to progressive drift in the estimated trajectory. To mitigate this issue, researchers have introduced physical priors to correct for errors. For instance, PDR [10] exploits the periodicity of human motion to detect gait and iteratively update the trajectory using estimated step length and heading. ZUPT [9], utilizing foot-mounted sensors, applies a zero-velocity constraint during stance phases to correct accumulated errors and improve accuracy in stationary conditions. Although these methods effectively suppress error propagation, their reliance on specific physical priors limits

their applicability to a narrow range of motion states and scenarios, reducing robustness in diverse environments.

Data-driven methods have demonstrated superior adaptability across diverse application scenarios, exhibiting greater robustness and improved accuracy compared to traditional approaches. For example, IONet [22] and RoNIN [11] disregard the IMU's mounting position and directly infer motion from raw measurements using a unified network framework, irrespective of how the device is worn. Specifically, RoNIN employs ResNet as the inference backbone; its robust localization performance and straightforward architecture have laid a solid foundation for subsequent research. Building on this, TLIO [15] and LIDR [23] integrate SCEKF and Invariant Extended Kalman Filter (LIEKF), respectively, to further refine ResNet's outputs and mitigate localization errors. RNIN-VIO [17] enhances the modeling of long-term dependencies by combining LSTM with ResNet.

In contrast, DIO contends that pose variations resulting from device placement are significant and introduces a novel pose-invariant inertial tracking loss, which regresses both the velocity magnitude and the trigonometric representation of the forward direction [24]. SC-HNN [25] and SSHNN [26] extend DIO by incorporating CNN and LSTM architectures augmented with CNN-based attention mechanisms. Similarly, RIO [2] and EqNIO [27] enrich the inference network with components designed to exploit rotational equivariance. More recently, CTIN [28] and iMOT [29] have explored the use of Transformer architectures for inertial localization, aiming to capture contextual dependencies, and have achieved promising

results.

Although increasingly complex network architectures have improved accuracy, they often suffer from reduced parameter efficiency, which poses significant challenges for deployment on resource-constrained devices, such as IoT platforms.

### B. Noise Cancellation Method

The accuracy of inertial sensor data directly impacts the precision of localization tasks. The noise model in inertial sensor measurements typically includes sensor bias and Gaussian white noise introduced during the measurement process [15]. The EKF is frequently employed to mitigate Gaussian white noise in inertial measurements, while filtering the trajectory estimates from neural networks can further reduce noise. An alternative approach is to apply EKF for fusing data from multiple sensor sources [30]–[32]. Additionally, significant progress has been made in applying neural networks for eliminating inertial measurement noise [33], [34]. Attention mechanisms are known for their superior ability to capture long-range dependencies compared to CNNs and LSTMs. However, conventional attention computes pairwise interactions between all queries and keys, regardless of their actual relevance. As a result, attention to irrelevant elements may introduce noise into the aggregated features, potentially degrading accuracy. This issue arises from the dense attention computation, which amplifies smaller similarity weights [35]. To address this, we propose a TSSA that preserves key attention values while discarding irrelevant components, thereby mitigating noise and improving localization accuracy.

## III. PROPOSED REPILN

This section presents the overall architecture of our Reparameterized Inertial Localization Network (RepILN). We describe the fundamental building block, the RepILN Block, which consists of two key components: the Reparameterization Module (RepBlock) and the Sparse Attention Gated Convolutional Unit (SA-GCU). The Temporal-Scale Sparse Attention (TSSA) mechanism serves as one branch within the SA-GCU.

### A. Overall Pipeline

The overall pipeline of the proposed RepILN, shown in Fig. 2(a), has a symmetric structure. Given an inertial measurement input  $\text{IMU} \in \mathbb{R}^{C \times L}$ , where  $C = 6$  represents three-axis accelerometer and gyroscope data, and  $L$  is the number of measurements per unit time (i.e., the sensor sampling rate), the RepBlock is applied at both the beginning and end of the backbone for channel alignment.

The network backbone consists of eight stacked RepILN Blocks, organized into four stages for rich motion information extraction. Each stage utilizes distinct channel and temporal dimensions, with downsampling achieved by adjusting convolutional strides and output dimensions in the final RepILN Block of the stage. Each RepILN Block comprises a reparameterization module (RepBlock) and a sparse attention gated convolutional unit (SA-GCU). Each RepBlock employs a multi-branch structure to extract complex motion patterns.

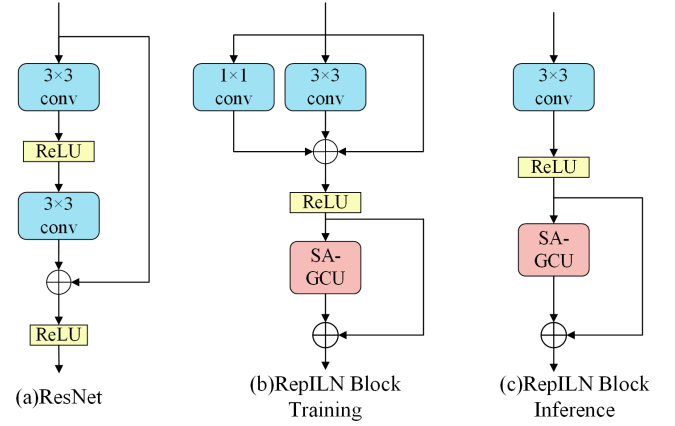


Fig. 3. Comparison of the basic modules of RepILN and ResNet. RepILN adopts a ResNet-like architecture during training, but reparameterizes the structure during inference to improve parameter efficiency.

During inference, this structure is reparameterized into a single-path feedforward form to improve parameter efficiency, shown in Fig. 2(c). Feature fusion is followed by the SA-GCU, which incorporates the TSSA mechanism, shown in Fig. 2(d). This mechanism captures long-term dependencies and discards irrelevant elements to mitigate noise. The extracted dependencies are then fused with local fine-grained motion features to enable multi-scale feature interaction. Skip connections are also integrated to bridge consecutive intermediate features, ensuring stable training and inference.

Finally, a multi-layer perceptron (MLP) head network outputs the predicted velocity, with the result obtained by minimizing the mean squared error (MSE) loss.

### B. Reparameterized Inertial Localization Module

To enhance parameter efficiency and facilitate deployment, we adopt reparameterization techniques in the design of the RepILN Block. Given an input  $X \in \mathbb{R}^{C \times L}$ , where  $C$  is the number of channels and  $L$  is the measurement length, the RepILN Block is defined as follows:

$$X' = \text{RepBlock}(X) \quad (1)$$

$$X'' = X' + \text{SA-GCU}(X') \quad (2)$$

Here,  $X'$  and  $X''$  represent the outputs of the RepBlock and the SA-GCU, respectively.

**Reparameterization Module(RepBlock).** To enhance parameter efficiency and extract rich motion features, the RepBlock decouples the training and inference architectures [36]. Fig. 3 illustrates the structural differences between the RepBlock and the basic block used in RoNIN ResNet. During training, a multi-branch architecture, similar to that of ResNet, is employed to extract features from inertial measurement data. Specifically, the training process for each RepBlock is defined as follows:

$$y = x + \phi(x) + \psi(x) \quad (3)$$

where  $x$  represents the input features,  $\phi(\cdot)$  and  $\psi(\cdot)$  denote 1D convolutional branches with kernel sizes of 3 and 1, respectively.

TABLE I  
OVERALL TRAJECTORY PREDICTION ACCURACY OF DIFFERENT MODELS. THE BEST-PERFORMING OUTCOMES HIGHLIGHTED IN BOLD.

Dataset	Metric	RoNIN ResNet	RoNIN-LSTM	RNIN	IMUNet	sTLIO	RepILN	RepILN Improvement over RoNIN ResNet
		Performance (meters)						
RoNIN	ATE	4.043	6.070	7.352	4.093	11.778	<b>3.939</b>	2.59%
	RTE	3.123	3.588	3.420	2.859	3.856	<b>2.857</b>	8.50%
RIDI	ATE	1.987	5.208	2.259	2.180	2.347	<b>1.718</b>	13.54%
	RTE	2.125	5.540	2.426	2.366	2.291	<b>1.927</b>	9.33%
RNIN-VIO	ATE	2.089	3.057	2.364	2.010	1.970	<b>1.875</b>	10.25%
	RTE	1.819	3.264	2.536	1.876	1.785	<b>1.731</b>	4.82%
TLIO	ATE	1.601	2.144	1.653	1.609	2.442	<b>1.459</b>	8.85%
	RTE	3.968	5.263	4.132	4.113	6.799	<b>3.637</b>	8.33%

During inference, the multi-branch structure is reparameterized into a single-path connection, shown in Fig. 3(c). This transformation preserves the equivalence of the learned parameters while simplifying the architecture, thus balancing computational efficiency with accuracy. For an inference-stage input  $x'$ , the process is abstracted as follows:

$$y' = \gamma(x') \quad (4)$$

where  $\gamma(x')$  represents a 1D convolution with a kernel size of 3, obtained by merging the parameters of  $\phi(\cdot)$ ,  $\psi(\cdot)$ , and the residual connection from the training stage. For consistency, the module output is defined as  $X' = \text{RepBlock}(X)$ .

**Temporal-Scale Sparse Attention (TSSA).** We first review the conventional attention mechanism, which captures long-term dependencies in the data [37]. Given an input  $X' \in \mathbb{R}^{C \times L}$ , it is transformed into queries  $Q$ , keys  $K$ , and values  $V$  through convolution or linear projection. Standard dot-product attention is computed as follows:

$$\text{Self-Attention} = \text{Softmax} \left( \frac{QK^T}{\alpha} \right) V \in \mathbb{R}^{C \times L} \quad (5)$$

where  $\alpha$  is a scaling factor, and the computational complexity is  $\mathcal{O}(LC^2)$ . This mechanism computes similarities across all key-query pairs, potentially incorporating irrelevant information and introducing noise.

In our approach, self-attention is applied along the temporal dimension to capture long-term trajectory dependencies while filtering out irrelevant elements to mitigate noise. For an input  $x$ , we generate keys  $K$ , queries  $Q$ , and values  $V$  by applying a 1D convolution with a kernel size of 1, followed by a depthwise 1D convolution with a kernel size of 3. To capture long-term dependencies, we compute  $\frac{K^T Q}{\alpha} \in \mathbb{R}^{L \times L}$ , which encapsulates dependencies among all key-query pairs. We then adopt a max- $e$  strategy, retaining only the max  $e\%$  elements in each row of  $\frac{K^T Q}{\alpha}$  (with  $e$  determined experimentally) and discarding the rest. Unlike random dropout, this approach selectively sparsifies the dependency matrix [35].

Finally, the sparsified dependency matrix is normalized and combined with the values  $V$  to yield the attention output:

$$TSSA = V \cdot \text{Softmax} \left( \max\text{-}e \left( \frac{K^T Q}{\alpha} \right) \right) \in \mathbb{R}^{C \times L} \quad (6)$$

Applying attention along the temporal dimension notably reduces the computational complexity to  $\mathcal{O}(CL^2)$ . As the network deepens and the channel dimension  $C$  increases, this reduction becomes significant, enhancing the inference efficiency of the inertial localization network.

**Sparse Attention Gate Convolutional Unit (SA-GCU):** The Gated Linear Unit (GLU) is a commonly employed mechanism for channel mixing [38]. In contrast, our proposed SA-GCU, as illustrated in Fig. 2(d), utilizes convolutional transformations for input processing. The gating branch employs a depthwise convolution followed by an activation function to capture local motion variations. This process forms a gated channel attention mechanism, enhancing fine-grained feature perception that TSSA alone may lack. Meanwhile, TSSA serves as the value branch, capturing long-term trajectory dependencies while filtering out irrelevant, noise-inducing elements. The outputs of these two branches are fused through a gating mechanism, facilitating multi-scale feature integration and enhancing the modeling of complex trajectory variations. The lightweight design of the SA-GCU ensures computational efficiency, making it a versatile mixer suitable for various inertial localization tasks.

## IV. EXPERIMENTS AND ANALYSIS

### A. Experimental settings

**Training details.** In this section, we compare the proposed RepILN against popular open-source data-driven baselines. All experiments, including both training and inference, are performed on an NVIDIA RTX 3090 GPU with 24 GB of memory. A Docker image encapsulating the runtime environment is made publicly available in the code repository. The training process adopts the Adam optimizer, with the initial learning rate set to  $10^{-4}$ . Training is run for a maximum of 100 epochs, with early stopping applied when the learning rate decays below  $10^{-6}$  to prevent overfitting.

**Datasets.** Four widely-used public benchmark datasets are employed for evaluation: RIDI, RoNIN, RNIN-VIO (which includes the 20-hour IDOL dataset), and TLIO. These datasets encompass a variety of carrying configurations, including handheld, pocket-mounted, and cart-based scenarios, as well as a wide range of indoor and outdoor acquisition environments. Notably, the TLIO dataset spans 60 hours, making it, to the

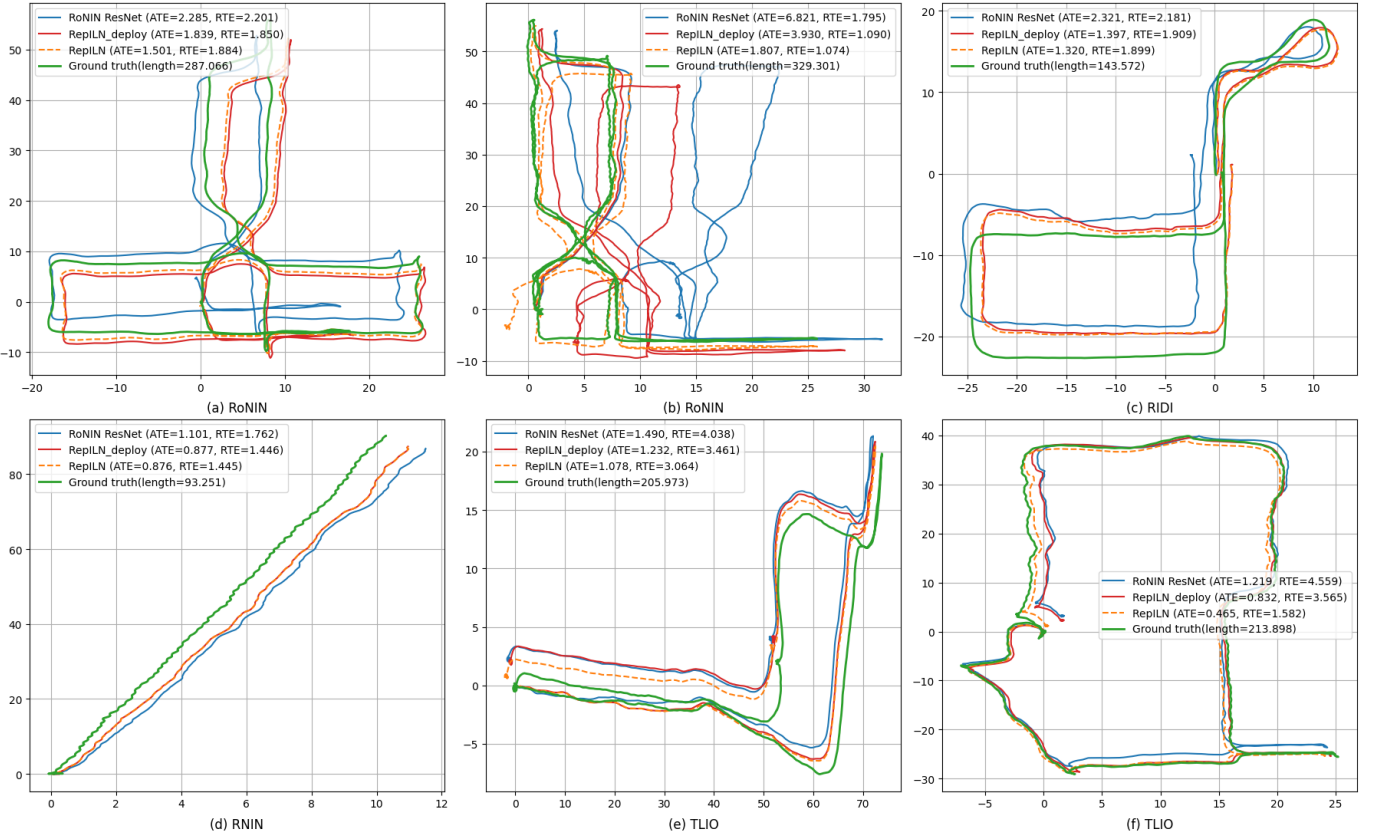


Fig. 4. Test data sample trajectories from the RoNIN, RIDI, RNIN, and TLIO datasets, along with the performance of all current state-of-the-art networks. The units of the X-axis and Y-axis are in meters. The numbers in parentheses indicate the ATE and RTE errors (in meters) and the total length of the test trajectory (in meters). All axes are measured in meters. Subscripts indicate the dataset to which each trajectory belongs. Note that the trajectories of ReplLN and ReplLN\_deploy may overlap due to their similar performance, resulting in partial occlusion of lines.

best of our knowledge, the longest publicly available inertial positioning benchmark to date. Each dataset is divided into training, validation, and testing sets using an 8:1:1 split ratio.

**Comparison of Methods.** Extensive research has demonstrated that data-driven approaches generally outperform Newtonian model-based methods in terms of localization accuracy [5], [11], [15], [17], [22], [39]–[43]. Accordingly, a set of representative open-source data-driven methods were selected as baselines for comparison. To ensure a fair evaluation, all baseline models were retrained on each respective dataset. We adopted the original implementations of the ResNet from RoNIN and transplanted its output module into the RoNIN LSTM framework to ensure that all baseline models maintain identical output specifications [11]. TLIO employs ResNet to estimate displacement and predict uncertainty, followed by a SCEKF for post-processing [15]. However, since TLIO relies on specific data collection protocols, it is incompatible with certain datasets. To address this limitation, we implemented only its neural network component, referred to as simplified TLIO (sTLIO) [26]. RNIN-VIO enhances the temporal modeling capability of ResNet by incorporating an LSTM module and was originally developed as part of a VIO system. As the open-source datasets used in this study do not contain visual data, we evaluate only its neural network component, denoted as simplified RNIN (RNIN) [17]. IMUNet adopts a

lightweight architecture based on depthwise separable convolutions, making it particularly well-suited for deployment on mobile devices. In our experiments, we used the original implementation of IMUNet without modification [18].

**Evaluation Metrics.** We use three common trajectory evaluation metrics to assess our model’s localization accuracy:

- **Absolute Trajectory Error (ATE)** quantifies the global trajectory consistency by computing the root mean square error (RMSE) between the predicted and ground truth trajectories over the entire sequence [44].
- **Relative Trajectory Error (RTE)** measures the local trajectory drift by computing the RMSE between the predicted and ground truth trajectories over fixed time intervals, set to 60 seconds in our evaluation [44].

## B. Results Analysis

**Metric Evaluation.** Table I presents the results of comparative experiments conducted on public datasets, with the best-performing outcomes highlighted in bold. The findings indicate that, in most scenarios, ReplLN achieves lower ATE and RTE. Compared to the traditional RoNIN ResNet model, ReplLN reduces ATE by 2.59% to 13.54% and RTE by 4.82% to 9.33% across four datasets.

With the evolution from RoNIN and sTLIO to RNIN, researchers have progressively increased model complexity in

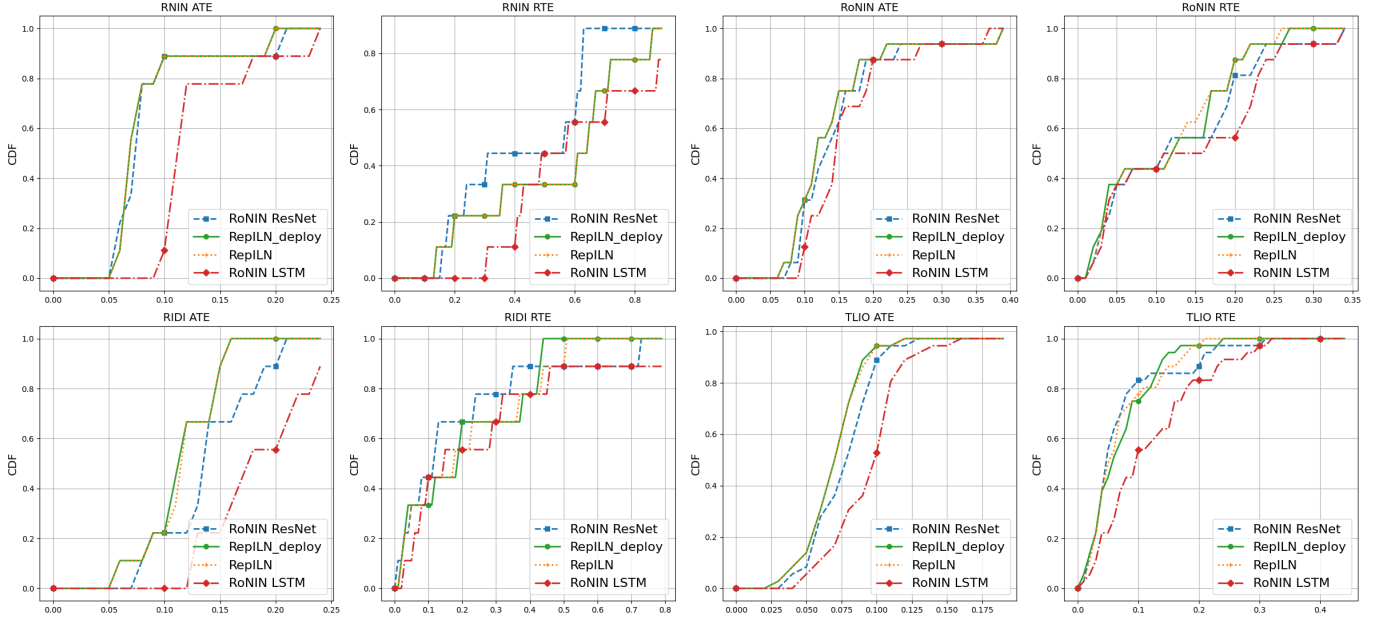


Fig. 5. Performance comparison of RepILN, RepILN\_deploy, RoNIN ResNet, and RoNIN-LSTM on the RNIN, RoNIN, RIDI, and TLIO datasets. For each dataset, three subplots are presented: the cumulative distribution functions (CDFs) of ATE and RTE. Note that the trajectories of RepILN and RepILN\_deploy may overlap due to their similar performance, resulting in partial occlusion of lines.

an effort to improve inertial localization accuracy. However, this improvement often comes at the expense of parameter efficiency, presenting challenges for deployment in IoT devices and other edge computing scenarios. Moreover, these models continue to exhibit limitations in modeling long-term trajectory dependencies, thereby constraining their performance. IMUNet, a lightweight model based on DSC, is similarly limited in its ability to model long-term dependencies, which restricts its overall localization performance. Additionally, DSC introduces higher memory access overhead, further reducing efficiency.

In contrast, the proposed RepILN addresses these challenges through a combination of architectural innovations. The decoupling of training and inference phases enhances parameter efficiency without compromising localization accuracy, thus achieving a balance between computational speed and precision—this aspect is elaborated upon in the ablation study. Furthermore, the introduction of the TSSA mechanism enables RepILN to effectively capture long-term dependencies while filtering out irrelevant components, thereby mitigating implicit noise interference. The SA-GCU further integrates local motion features with long-range dependencies, promoting multi-scale feature interactions.

Overall, these advancements collectively provide a compelling explanation for RepILN's superior performance compared to baseline models.

**Visualization.** Fig. 4 presents representative sample trajectories from the test sets of various datasets, encompassing both complex rotational and near-linear motion patterns. In the near-linear scenario (Fig. 4(d)), RepILN successfully captures long-term dependencies, enabling accurate and stable trajectory tracking. Following the reparameterization of RepILN into an inference-friendly architecture, the resulting model—denoted

as RepILN\_deploy—continues to achieve higher accuracy than the RoNIN ResNet baseline. This indicates that the accuracy degradation caused by the reparameterization process remains within acceptable bounds. For complex trajectories (Figs. 4(a), (b), (c), (e), and (f)), RepILN exhibits strong proficiency in modeling local motion variations, especially in rotational segments. This capability allows both RepILN and RepILN\_deploy to closely follow the ground-truth trajectories, which leads to significantly lower ATE and RTE values under nonlinear motion conditions. In contrast, RoNIN ResNet increasingly diverges from the ground truth as the complexity of the trajectory grows. The enhanced ability of RepILN and RepILN\_deploy to model long-term dependencies contributes to maintaining overall trajectory consistency, though minor heading drift may still occur in certain segments.

**Model Performance Evaluation.** The cumulative distribution functions (CDFs) of ATE and RTE for each network on the test sequences are presented in Fig. 5. The steeper slopes of the green and orange curves, representing RepILN and RepILN\_deploy respectively, indicate faster error convergence and overall lower ATE and RTE values compared to the RoNIN variants. Overall, RepILN and RepILN\_deploy consistently outperform the benchmark models, demonstrating superior accuracy and reliability in inertial localization tasks.

### C. Ablation Study

This section evaluates the effectiveness of each model component through ablation experiments. It also analyzes the changes in localization accuracy and model complexity introduced by the reparameterization process.

**Effectiveness of Model Components.** We design two model variants: the complete RepILN model incorporating the SA-GCU module (which includes the TSSA mechanism),

TABLE II

OVERVIEW OF THE ABLATION STUDY. WE ABLATE THE SA-GCU MODULE, WHICH CONTAINS TSSA, FROM REPILN TO EVALUATE THE EFFECTIVENESS OF BOTH THE REPARAMETERIZATION TECHNIQUE AND SA-GCU. THE BEST RESULT IS SHOWN IN BOLD FONT. ALL THE METRICS ARE IN METERS.

Models	RepBlock	SA-GCU	RoNIN		RIDI		RNIN-VIO		TLIO	
			ATE	RTE	ATE	RTE	ATE	RTE	ATE	RTE
Baseline(RoNIN-resnet18)	–	–	4.043	3.123	1.987	2.125	2.089	1.819	1.601	3.968
RepILN (w/o SA-GCU)	✓	–	4.288	3.175	1.860	1.990	2.085	1.802	1.560	3.916
RepILN (w SA-GCU)	✓	✓	<b>3.939</b>	<b>2.857</b>	<b>1.718</b>	<b>1.927</b>	<b>1.875</b>	<b>1.731</b>	<b>1.459</b>	<b>3.637</b>

TABLE III

RE-PARAMETERIZATION PERFORMANCE COMPARISON ON THE RNIN-VIO DATASET. THE BEST RESULT IS SHOWN IN BOLD FONT.

Dataset	Metric	RoNIN ResNet	RepILN	RepILN_deploy
RNIN-VIO	ATE (meter)	2.089	<b>1.875</b>	1.876
	RTE (meter)	1.875	<b>1.731</b>	1.732
\	FLOPs (M)	<b>38.252</b>	60.968	76.784
	Parameters (M)	4.635	4.456	<b>3.809</b>

denoted as RepILN (w SA-GCU), and a simplified version without the SA-GCU module, denoted as RepILN (w/o SA-GCU). The RepBlock serves as the shared backbone and is retained in both variants.

Table II summarizes the ablation results across four public datasets. RoNIN ResNet is included as a baseline for comparison. Even without the SA-GCU module, RepILN (w/o SA-GCU) remains capable of effectively capturing motion features, achieving significantly lower localization errors compared to RoNIN ResNet. This demonstrates the effectiveness of the reparameterized structure in learning and modeling motion representations during training. However, the absence of the SA-GCU module limits the model’s ability to capture long-term trajectory dependencies, leading to a reduction in overall localization accuracy.

Despite this trade-off, the substantially reduced number of parameters in RepILN (w/o SA-GCU) makes it well-suited for deployment in resource-constrained environments, such as IoT devices. In contrast, RepILN (w SA-GCU), which includes both the full reparameterized architecture and the SA-GCU module, achieves further improvements in localization accuracy compared to its simplified counterpart. This highlights the importance of multi-scale feature fusion provided by the SA-GCU module in enhancing trajectory estimation.

**Effectiveness of Model Reparameterization.** During inference, the multi-branch training architecture is reparameterized into a single-path feedforward network. This transformation allows the model to preserve most of its performance observed during training while significantly reducing the number of parameters, thus improving its suitability for deployment on resource-constrained IoT devices. Fig. 4 provides a visual comparison between the original training network (RepILN) and the reparameterized inference network (RepILN\_deploy) in terms of trajectory reconstruction.

To further quantify the impact of reparameterization on localization accuracy and model complexity, a detailed analysis is presented in Table III. The results show that RepILN (w

SA-GCU) achieves higher localization accuracy with fewer parameters (4.456M) compared to RoNIN-ResNet(4.635M), demonstrating its efficiency and deployability on embedded platforms.

After reparameterization, RepILN\_deploy (3.809M parameters) reduces the parameter count by approximately 14.52% compared to RepILN (4.456M parameters), and its model size is only 82.18% of that of RoNIN-ResNet (4.635M parameters). Despite this compression, RepILN\_deploy exhibits an increase of only 0.001 meters in both ATE and RTE. Importantly, it continues to outperform RoNIN-ResNet in terms of localization accuracy. These findings demonstrate that the proposed model effectively balances computational efficiency with localization precision, making it particularly suitable for IoT devices and mobile platforms with limited computing resources. They also underscore the critical role of each architectural component in enhancing inertial localization performance.

## V. CONCLUSION

In this work, we propose a decoupled training and inference framework that enhances parameter efficiency while striking a balance between computational cost and localization accuracy. With fewer parameters than RoNIN ResNet, our method achieves the lowest localization error across benchmarks, offering an effective and lightweight inertial localization solution for IoT devices with constrained computational resources. Despite these improvements, the issue of accumulated heading drift remains an open challenge. Future work will explore the integration of adaptive correction mechanisms to further enhance long-term localization stability and robustness in real-world applications.

## REFERENCES

- [1] D. Engelsman and I. Klein, “Information-aided inertial navigation: A review,” *IEEE Transactions on Instrumentation and Measurement*, vol. 72, no. 8507418, 2023.
- [2] X. Cao, C. Zhou, D. Zeng, and Y. Wang, “Rio: Rotation-equivariance supervised learning of robust inertial odometry,” in *2022 IEEE/CVF Conference on Computer Vision and Pattern Recognition (CVPR)*, 2022, pp. 6604–6613.
- [3] S. Herath, D. Caruso, C. Liu, Y. Chen, and Y. Furukawa, “Neural inertial localization,” in *Proceedings of the 2022 IEEE/CVF Conference on Computer Vision and Pattern Recognition (CVPR)*, 2022, pp. 6594–6603.
- [4] —, “Neural inertial localization,” in *2022 IEEE/CVF Conference on Computer Vision and Pattern Recognition (CVPR)*, 2022, pp. 6594–6603.
- [5] A. K. Panja, C. Chowdhury, and S. Neogy, “Survey on inertial sensor-based ils for smartphone users,” *CCF Transactions on Pervasive Computing and Interaction*, vol. 4, no. 3, pp. 319–337, 2022.

- [6] B. Zhou, P. Wu, X. Zhang, D. Zhang, and Q. Li, "Activity semantics-based indoor localization using smartphones," *IEEE Sensors Journal*, vol. 24, no. 7, pp. 11 069–11 079, 2024.
- [7] M. Freyding and B. Or, "Learning car speed using inertial sensors for dead reckoning navigation," *IEEE Sensors Letters*, vol. 6, no. 9, pp. 1–4, 2022.
- [8] P. G. Savage, "Strapdown inertial navigation integration algorithm design part 2: Velocity and position algorithms," *Journal of Guidance, Control, and Dynamics*, vol. 21, no. 2, pp. 208–221, 1998.
- [9] R. P. Suresh, V. Sridhar, J. Pramod, and V. Talasila, "Zero velocity potential update (zupt) as a correction technique," in *Proceedings of the 2018 3rd International Conference On Internet of Things: Smart Innovation and Usages (IoT-SIU)*, 2018, pp. 1–8.
- [10] A. Nayak, A. Eskandarian, Z. Doerzaph, and P. Ghorai, "Pedestrian trajectory forecasting using deep ensembles under sensing uncertainty," *IEEE Transactions on Intelligent Transportation Systems*, vol. 25, no. 9, pp. 11 317–11 329, 2024.
- [11] S. Herath, H. Yan, and Y. Furukawa, "Ronin: Robust neural inertial navigation in the wild: Benchmark, evaluations, & new methods," in *2020 IEEE International Conference on Robotics and Automation (ICRA)*, 2020, pp. 3146–3152.
- [12] K. He, X. Zhang, S. Ren, and J. Sun, "Deep residual learning for image recognition," in *Proceedings of the 2016 IEEE Conference on Computer Vision and Pattern Recognition (CVPR)*, 2016, pp. 770–778.
- [13] S. Hochreiter and J. Schmidhuber, "Long short-term memory," *Neural Computation*, vol. 9, no. 8, pp. 1735–1780, 1997.
- [14] C. Lea, R. Vidal, A. Reiter, and G. D. Hager, "Temporal convolutional networks: A unified approach to action segmentation," in *Computer Vision – ECCV 2016 Workshops*, G. Hua and H. Jégou, Eds. Cham: Springer International Publishing, 2016, pp. 47–54.
- [15] W. Liu, D. Caruso, E. Ilg, J. Dong, A. I. Mourikis, K. Daniilidis, V. Kumar, and J. Engel, "Tlio: Tight learned inertial odometry," *IEEE Robotics and Automation Letters*, vol. 5, no. 4, pp. 5653–5660, 2020.
- [16] S. Roumeliotis and J. Burdick, "Stochastic cloning: a generalized framework for processing relative state measurements," in *Proceedings 2002 IEEE International Conference on Robotics and Automation (Cat. No.02CH37292)*, vol. 2, 2002, pp. 1788–1795 vol.2.
- [17] D. Chen, N. Wang, R. Xu, W. Xie, H. Bao, and G. Zhang, "Rnnvio: Robust neural inertial navigation aided visual-inertial odometry in challenging scenes," in *2021 IEEE International Symposium on Mixed and Augmented Reality (ISMAR)*, 2021, pp. 275–283.
- [18] B. Zeinali, H. Zanddizari, and M. J. Chang, "Imunet: Efficient regression architecture for inertial imu navigation and positioning," *IEEE Transactions on Instrumentation and Measurement*, vol. 73, no. 2516213, 2024.
- [19] A. G. Howard, M. Zhu, B. Chen, D. Kalenichenko, W. Wang, T. Weyand, M. Andreetto, and H. Adam, "Mobilenets: Efficient convolutional neural networks for mobile vision applications," 2017.
- [20] M. Tan, B. Chen, R. Pang, V. Vasudevan, M. Sandler, A. Howard, and Q. V. Le, "Mnasnet: Platform-aware neural architecture search for mobile," in *Proceedings of the IEEE/CVF conference on computer vision and pattern recognition*, 2019, pp. 2820–2828.
- [21] M. Tan and Q. Le, "Efficientnet: Rethinking model scaling for convolutional neural networks," in *International conference on machine learning*. PMLR, 2019, pp. 6105–6114.
- [22] C. Chen, X. Lu, A. Markham, and N. Trigoni, "Ionet: Learning to cure the curse of drift in inertial odometry," in *Proceedings of the AAAI Conference on Artificial Intelligence*, vol. 32, no. 1, 2018.
- [23] D. Yang, H. Liu, X. Jin, J. Chen, C. Wang, X. Ding, and K. Xu, "Enhancing vio robustness under sudden lighting variation: A learning-based imu dead-reckoning for uav localization," *IEEE Robotics and Automation Letters*, vol. 9, no. 5, pp. 4535–4542, 2024.
- [24] Y. Wang, H. Cheng, C. Wang, and M. Q.-H. Meng, "Pose-invariant inertial odometry for pedestrian localization," *IEEE Transactions on Instrumentation and Measurement*, vol. 70, no. 8503512, 2021.
- [25] Y. Wang, H. Cheng, and M. Q.-H. Meng, "Spatiotemporal co-attention hybrid neural network for pedestrian localization based on 6d imu," *IEEE Transactions on Automation Science and Engineering*, vol. 20, no. 1, pp. 636–648, 2023.
- [26] Y. Wang, H. Cheng, A. Zhang, and M. Q.-H. Meng, "From imu measurement sequence to velocity estimate sequence: An effective and efficient data-driven inertial odometry approach," *IEEE Sensors Journal*, vol. 23, no. 15, pp. 17 117–17 126, 2023.
- [27] R. K. Jayanth, Y. Xu, Z. Wang, E. Chatzipantazis, K. Daniilidis, and D. Gehrig, "EqNIO: Subequivariant neural inertial odometry," in *The Thirteenth International Conference on Learning Representations*, 2025. [Online]. Available: <https://openreview.net/forum?id=C8jXEugWkq>
- [28] B. Rao, E. Kazemi, Y. Ding, D. M. Shila, F. M. Tucker, and L. Wang, "Ctin: Robust contextual transformer network for inertial navigation," *Proceedings of the AAAI Conference on Artificial Intelligence*, vol. 36, no. 5, pp. 5413–5421, Jun. 2022. [Online]. Available: <https://ojs.aaai.org/index.php/AAAI/article/view/20479>
- [29] S. M. Nguyen, L. D. Tran, D. Viet Le, and P. J. M. Havinga, "iMoT: Inertial Motion Transformer for Inertial Navigation," *arXiv e-prints*, p. arXiv:2412.12190, Dec. 2024.
- [30] M. Zhang, X. Zuo, Y. Chen, Y. Liu, and M. Li, "Pose estimation for ground robots: On manifold representation, integration, reparameterization, and optimization," *IEEE Transactions on Robotics*, vol. 37, no. 4, pp. 1081–1099, 2021.
- [31] A. I. Mourikis and S. I. Roumeliotis, "A multi-state constraint kalman filter for vision-aided inertial navigation," in *Proceedings of the 2007 IEEE International Conference on Robotics and Automation*, 2007, pp. 3565–3572.
- [32] P. Geneva, K. Eickenhoff, and G. Huang, "A linear-complexity ekf for visual-inertial navigation with loop closures," in *2019 International Conference on Robotics and Automation (ICRA)*, 2019, pp. 3535–3541.
- [33] C. Jiang, S. Chen, Y. Chen, B. Zhang, Z. Feng, H. Zhou, and Y. Bo, "A mems imu de-noising method using long short-term memory recurrent neural networks (lstm-rnn)," *Sensors*, vol. 18, no. 10, p. 3470, 2018.
- [34] N. Cohen and I. Klein, "Inertial navigation meets deep learning: A survey of current trends and future directions," *Results in Engineering*, vol. 24, p. 103565, 2024. [Online]. Available: <https://www.sciencedirect.com/science/article/pii/S2590123024018085>
- [35] X. Chen, H. Li, M. Li, and J. Pan, "Learning a sparse transformer network for effective image deraining," in *Proceedings of the IEEE/CVF Conference on Computer Vision and Pattern Recognition (CVPR)*, June 2023, pp. 5896–5905.
- [36] X. Ding, X. Zhang, N. Ma, J. Han, G. Ding, and J. Sun, "Repvgg: Making vgg-style convnets great again," in *Proceedings of the IEEE/CVF Conference on Computer Vision and Pattern Recognition*, 2021, pp. 13 733–13 742.
- [37] A. Dosovitskiy, L. Beyer, A. Kolesnikov, D. Weissenborn, X. Zhai, T. Unterthiner, M. Dehghani, M. Minderer, G. Heigold, S. Gelly, J. Uszkoreit, and N. Houlsby, "An Image is Worth 16x16 Words: Transformers for Image Recognition at Scale," *arXiv e-prints*, p. arXiv:2010.11929, Oct. 2020.
- [38] D. Shi, "Transnext: Robust foveal visual perception for vision transformers," in *Proceedings of the IEEE/CVF Conference on Computer Vision and Pattern Recognition (CVPR)*, June 2024, pp. 17 773–17 783.
- [39] H. Yan, Q. Shan, and Y. Furukawa, "Ridi: Robust imu double integration," in *Computer Vision – ECCV 2018*, V. Ferrari, M. Hebert, C. Sminchisescu, and Y. Weiss, Eds. Cham: Springer International Publishing, 2018, pp. 641–656.
- [40] C. Chen, P. Zhao, C. X. Lu, W. Wang, A. Markham, and N. Trigoni, "Oxiod: The dataset for deep inertial odometry," *arXiv preprint arXiv:1809.07491*, 2018.
- [41] R. Harle, "A survey of indoor inertial positioning systems for pedestrians," *IEEE Communications Surveys & Tutorials*, vol. 15, no. 3, pp. 1281–1293, 2013.
- [42] C. Chen and X. Pan, "Deep learning for inertial positioning: A survey," *IEEE Transactions on Intelligent Transportation Systems*, vol. 25, no. 9, pp. 10 506–10 523, 2024.
- [43] C. L. Gentil, F. Tschopp, I. Alzugaray, T. Vidal-Calleja, R. Siegwart, and J. Nieto, "Idol: A framework for imu-dvs odometry using lines," 2020, arXiv:2008.05749.
- [44] J. Sturm, N. Engelhard, F. Endres, W. Burgard, and D. Cremers, "A benchmark for the evaluation of rgb-d slam systems," in *Proceedings of the 2012 IEEE/RSJ International Conference on Intelligent Robots and Systems*, 2012, pp. 573–580.